Strong-chaos-caused negative mobility in a periodic substrate potential

Yuhui Luo,[1,3] Chunhua Zeng,[1,*] and Bao-Quan Ai[2,†]

[1]*Faculty of Civil Engineering and Mechanics/Faculty of Science, Kunming University of Science and Technology, Kunming 650500, China*

[2]*Guangdong Provincial Key Laboratory of Quantum Engineering and Quantum Materials, GPETR Center for Quantum Precision Measurement, SPTE, South China Normal University, Guangzhou 510006, China*

[3]*College of Physics and Information Engineering, Zhaotong University, Zhaotong 657000, China*

(Received 5 June 2020; revised 15 September 2020; accepted 17 September 2020; published 12 October 2020)

We numerically investigate negative mobility of an inertial Brownian particle moving in a periodic double-well substrate potential in the presence of a time-periodic force and a constant bias. For the deterministic case, we find from the average velocity that the varying shape parameter and driving forces can cause negative mobility, differential negative mobility, and giant positive mobility. We analyze these findings via the bifurcation diagram and maximal Lyapunov exponent and find that certain chaos can give rise to negative mobility. For the presence of a Gaussian color noise, the results suggest that the noise intensity can enhance or result in negative and positive mobilities, whereas correlation time can enhance, weaken, or even eliminate them. On the basis of the time series, phase-space map, and power spectrum of various attractors, we unveil how these mobilities connect to strong chaotic attractors (SCAs), including both stable attractor and unstable attractors, and propose an underlying mechanism that SCAs can result in the negative mobility, whereas other attractors do not. Our findings may be potentially useful for research on anomalous transports of the particles and on designs of various devices, such as atomic chains, crystals with dislocations, and superconducting nanowires, etc.

DOI: 10.1103/PhysRevE.102.042114

I. INTRODUCTION

Understanding the dynamics of transport phenomena, the core of many problems in physics, chemistry, and biology [1], is an outstanding challenge in a system away from equilibrium. Because systems out of equilibrium can lead to the occurrence of paradoxical situations since the laws of thermodynamics no longer possess validity, many fundamental problems of these systems remain uncertain. Consequently, the occurrence of anomalous phenomena in these systems was extensively investigated in physics, chemistry, and biology. A typical example for biological system out of equilibrium is anomalous diffusions of the energy landscape in human chromosomes [2]. Intriguing examples for quantum systems far from equilibrium are directed transport of atoms in a quantum ratchet [1] and nonlinear transport in an out-of-equilibrium single-site Bose-Hubbard model [3]. Another example is absolute negative conductance (ANC) [4] and phase diffusion [5] in the Josephson junctions circuit. A striking example for a classical system far from equilibrium is absolute negative mobility (ANM), differential negative mobility (DNM) [4], and anomalous diffusions [6] in a symmetrical potential. In particular, negative mobility, which implies that the particle moves in a direction opposite to a small bias and is also called anomalous mobility, has been in the research spotlight [4,7–15] for 20 years. Much progress in both theoretical [4,7] and experimental [16] investigations has been made in ANM.

In fact, Brownian particles moving in a system driven by thermal fluctuation and external forces usually exhibit very complex transport behaviors, such as anomalous transports, collective motion, chaotic state, even vortices [17] or turbulent state [18,19]. Therefore numerous works [6,7,10–12,16,20] have focused on various anomalous mobilities since the late 1990s, but most of these works have frequently paid attention to the occurrence of the phenomena without providing the physical mechanism behind them. Actually, these anomalous transports may be caused by chaos. Notice that by using the bifurcation diagram, ANM has been investigated in a symmetrical periodic system [4], a repulsive Yukawa potential [8], and an inertial rocking system [9] and ANC in superconducting quantum interference device ratchet [5]. Furthermore, the negative mobility of a Brownian particle for strong damping regime was studied via maximal Lyapunov exponent (MLE) [21].

To our knowledge, still very little is known about various mobilities (e.g., ANM, DNM, etc.) and physical mechanisms behind them in a periodic double-well substrate potential, also called the Remoissenet-Peyrard substrate potential [22,23]. It is frequently used to describe the substrate in charge-density-wave conductors, Josephson junctions arrays, crystals with dislocations [24], hydrogen-bonded networks [25], superconducting nanowires [26], and kink-bearing systems [23]. It is well established that the on-site substrate potentials are usually assumed to be the cosinelike type potential. However, certain realistic substrate potentials are very complex and maybe possess the form of a periodic double-well substrate potential [24,27] in condensed matter physics, with a particular case of the sine-Gordon potential. Thus, since the

*zchh2009@126.com
†aibq@scnu.edu.cn

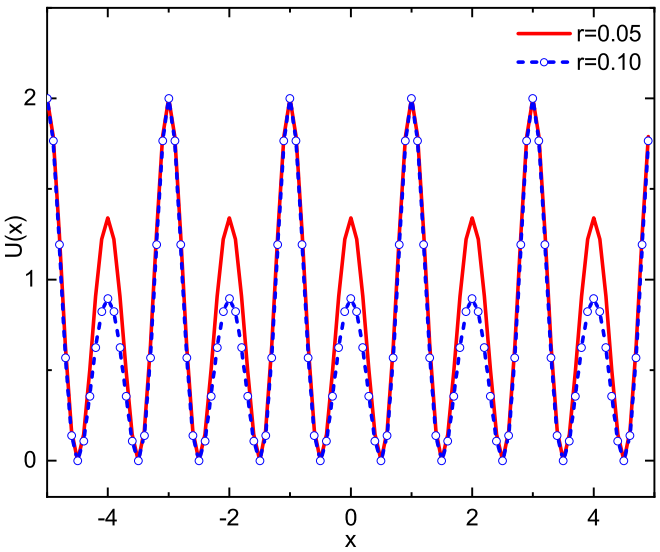

FIG. 1. The periodic double-well substrate potential for different shape parameters r.

early 1990s several works have focused on the anomalous phenomena of a system with the substrate potential, such as proton transport by solitons [25], the diffusion process [28], a rich spectrum of dynamical behaviors [29], etc. Additionally, similar anomalous behaviors had been studied in the Frenkel-Kontorova model with a deformable substrate potential, such as the dynamical-mode-locking phenomena [30], thermal conductivity, and negative differential thermal resistance [31]. Moreover, it is noteworthy that a periodic double-well substrate potential frequently exhibits localization of energy transport [32] since the potential consists of potential barriers with high and low dislocations, as shown in Fig. 1. Consequently, various localizations were extensively investigated in this type of disorder system [6,27]. In a word, the periodic double-well substrate potential with incommensurability plays a crucial role in atomic chains.

Moreover, numerous works usually investigated anomalous mobilities of the particle moving in systems with a thermal fluctuation modeled by a Gaussian white noise for the ideal case. However, a thermal fluctuation is a Gaussian color noise for the real case [33]. Based on the above, the aim of this paper is to examine the anomalous behaviors of a Brownian particle moving in the periodic double-well substrate potential driven by a time-periodic force and a constant bias. Via the bifurcation diagram, time series, phase-space map, power spectrum, and MLE, we analyze the relationships between dynamical behaviors and various mobilities and discuss the physical mechanisms behind them. It is worth mentioning that the periodic, quasiperiodic, and chaotic dynamics in simple gene elements were analyzed by the bifurcation diagram, phase-space map, and power spectrum in the recent work [34].

The rest of the paper is structured as follows. In Sec. II, we present the model and methodology in detail. In Sec. III, for the deterministic dynamics, various mobilities—specially anomalous mobility—are discussed via the average velocity. We analyze the reasons for these results by the bifurcation diagram and MLE. To better understand the physical mechanism hinted behind these phenomena, we also analyze these findings via the time series, the phase-space map, and the power spectrum. For the presence of a Gaussian color noise, the noise effects on anomalous transports are studied via the average velocity and mobility coefficient. Moreover, these findings are also analyzed via the time series, the phase-space map, and the power spectrum. Conclusions and applications are presented in Sec. IV.

II. THE MODEL

We consider an inertial Brownian particle with mass m moving in a periodic double-well substrate potential with a color thermal fluctuation and under the influence of an external constant bias F. To drive the system out of equilibrium, the potential is also driven by an external time-periodic force $a\sin(\omega t)$ with amplitude a and frequency ω. Thus the model is described by Langevin equation in the following form:

$$m\ddot{x} + \gamma\dot{x} = -V'(x) + F + a\sin(\omega t) + \eta(t), \qquad (1)$$

where the prime and dot are a differentiation with respect to coordinate x of the particle and time t, respectively. γ is the friction coefficient. The periodic double-well substrate potential is given by [22,27]

$$V(x) = \frac{(1-r)^4[1+\cos(2\pi x)]}{[1+r^2+2r\cos(\pi x)]^2},$$

where r is a shape parameter with range $-1 < r < 1$. In order to understand a sketch of the system, we present the shape of the potential for different shape parameters r in Fig. 1. $\eta(t)$ denotes a Gaussian colored noise due to thermal fluctuation of the system, and its correlation properties can be written as

$$\langle\eta(t)\rangle = 0,$$
$$\langle\eta(t)\eta(t')\rangle = \frac{D}{\tau_0}\exp\left(-\frac{|t-t'|}{\tau_0}\right),$$

where D denotes the noise intensity and τ_0 is correlation time. We fix $m = 1$, $\gamma = 0.9$, $a = 4.35$, and $\omega = 4.86$, unless otherwise stated. All quantities are in dimensionless units.

The Fokker-Planck equation corresponding to Langevin equation (1) cannot be commonly solved, and therefore we study the system by numerical simulation. To ensure reliable results, the Eq. (1) is integrated by a fourth-order Runge-Kutta scheme [35] with time step $\triangle t = 10^{-2}$. The average velocity and mobility coefficient are calculated through 500 different trajectories, whose initial positions $x(t=0)$ and velocities $v(t=0)$ are uniformly distributed over the intervals $[-1, 1]$ and $[-0.5, 0.5]$, respectively. The first 10^6 data of these trajectories are discarded to remove initial transient states, and then their 10^7 data are used to calculate the average velocity and the mobility coefficient. The data of a single trajectory [whose initial position $x(t=0)$ and velocity $v(t=0)$ are 0.1 and 0.0, respectively] are used to plot the bifurcation diagram, time series, and the phase-space map and to compute the power spectrum and the MLE. The first 10^6 data of the trajectory are discarded to remove initial transient states. Then we use its 10^4–10^5 data of the steady state to plot the phase-space map and the time series. Moreover, 2^{14} data of the steady state of the single trajectory are used to calculate the power

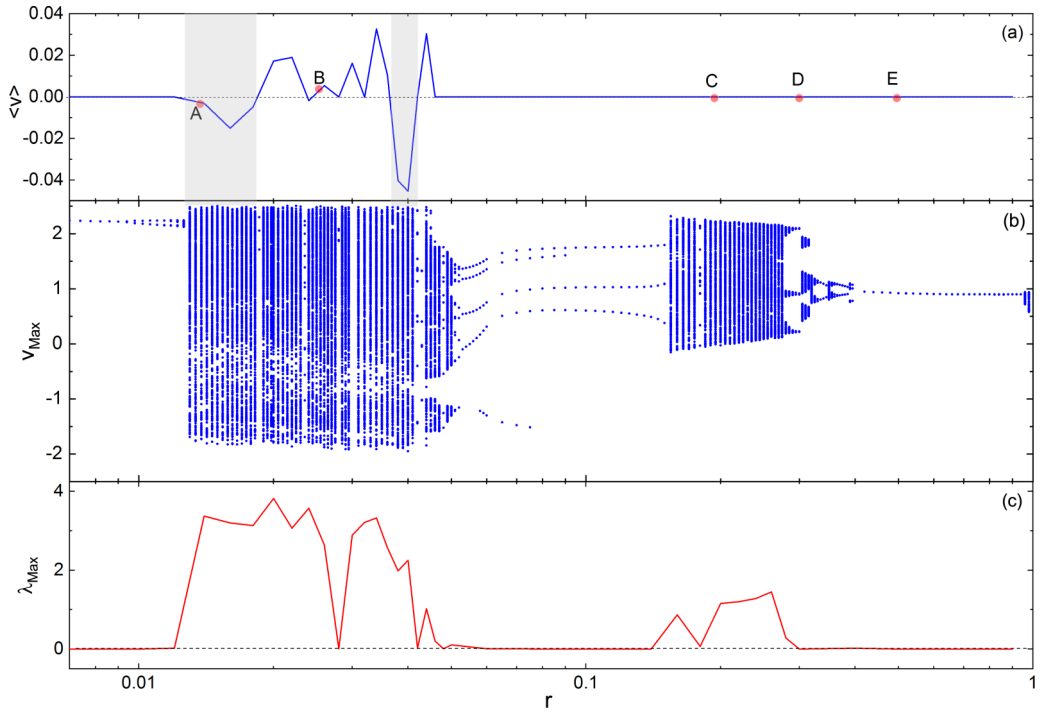

FIG. 2. The average velocity (a), the bifurcation diagram (b), and the MLE (c) vs. the shape parameter r in the absence of noise ($D = 0$). The other parameter is $F = 0.05$. The points A–E referenced in Fig. 3.

spectrum and the MLE. Here the the power spectrum is defined by $P = |g(w)|^2$, where $g(w) = \frac{1}{\sqrt{2\pi}} \int_{-\infty}^{\infty} v(t) e^{i\omega t} dt$. And the Lyapunov exponent is computed numerically using the algorithm proposed by Wolf *et al*. [36]. Notice that the MLE $\lambda_{\text{Max}} > 0$ denotes chaotic behavior. The larger the MLE, the more chaotic the system. And $\lambda_{\text{Max}} \simeq 0$ presents no chaos, namely the system is exhibiting some sort of orbital stability or periodicity.

III. RESULTS AND DISCUSSIONS

A. The deterministic dynamics

We first focus on the case of the deterministic dynamics ($D = 0$). To gain an understanding of how the shape parameter of the system r affects the particle's mobility, we present the average velocity, the bifurcation diagram of the velocity, and the MLE versus the shape parameter r in Fig. 2. Figure 2(a) shows that average velocities are zero except for the range of $r = 0.014$ to 0.045. It should be noted that there exist two times negative mobilities with increasing shape parameter r (gray). Moreover, Fig. 2(b) shows that the varying shape parameter r can cause double-periodic bifurcation, chaotic bands, periodic windows, and attractor-merging crisis. It is of great importance that the regime of the existence of nonzero average velocities corresponds to the chaotic band in the bandwidth range of $r = 0.014$ to 0.045.

To further verify chaotic behaviors, the MLE λ_{Max} as a function of r is plotted in Fig. 2(c). The nonzero average velocities in Fig. 2(a) obviously correspond to the large and positive MLEs in Fig. 2(c). This finding suggests that the nonzero mobilities may be caused by chaos. Contrasting the bifurcation diagram with the MLE, we find that the chaotic bands in Fig. 2(b) clearly correspond to the positive MLEs in Fig. 2(c). Moreover, it is worthwhile mentioning that the zero average velocities in Fig. 2(a) correspond to nonchaotic bands and the rest chaotic bands in Fig. 2(b) or to $\lambda_{\text{Max}} \simeq 0$ and small MLEs in Fig. 2(c). In fact, the periodic attractor corresponds to trivial negative MLE in the figure. In other words, this brings up the question of why certain chaos can result in the nonzero average velocity while the rest does not, which will be discussed below. In other words, the result suggests that certain chaos may result in the occurrence of negative mobility.

The question is still open that certain chaos can result in the occurrence of the nonzero average velocity whereas the rest does not. To answer this question, we analyze these findings via the time series, the phase-space map, and the power spectrum in Fig. 3. When $r = 0.014$ (the A column), the dynamical behaviors are the following. First, the time series of position displays that the continuous hoppings of the particle from a double well to another adjacent double well are observed in the negative direction of the axis x. Second, the time series of velocity shows irregularity. Third, the map is irregular and shows that the trajectory leaves stable attractor (initial double well) and continuously forms new unstable attractors in other double wells in the negative direction of the axis x. Additionally, the spectrum has dominated by downward spikes. Thus the attractors corresponding to $r = 0.014$ are of strong chaotic attractors (SCAs) [34]. Moreover, Fig. 2(a) shows that the average velocity corresponding to $r = 0.014$ is negative, implying that SCAs can cause negative mobility. For $r = 0.026$ (the B column), the corresponding dynamical behaviors are as follows. First, the time series of the position displays that the hoppings of the particle from a double well to another adjacent double well are observed in the positive

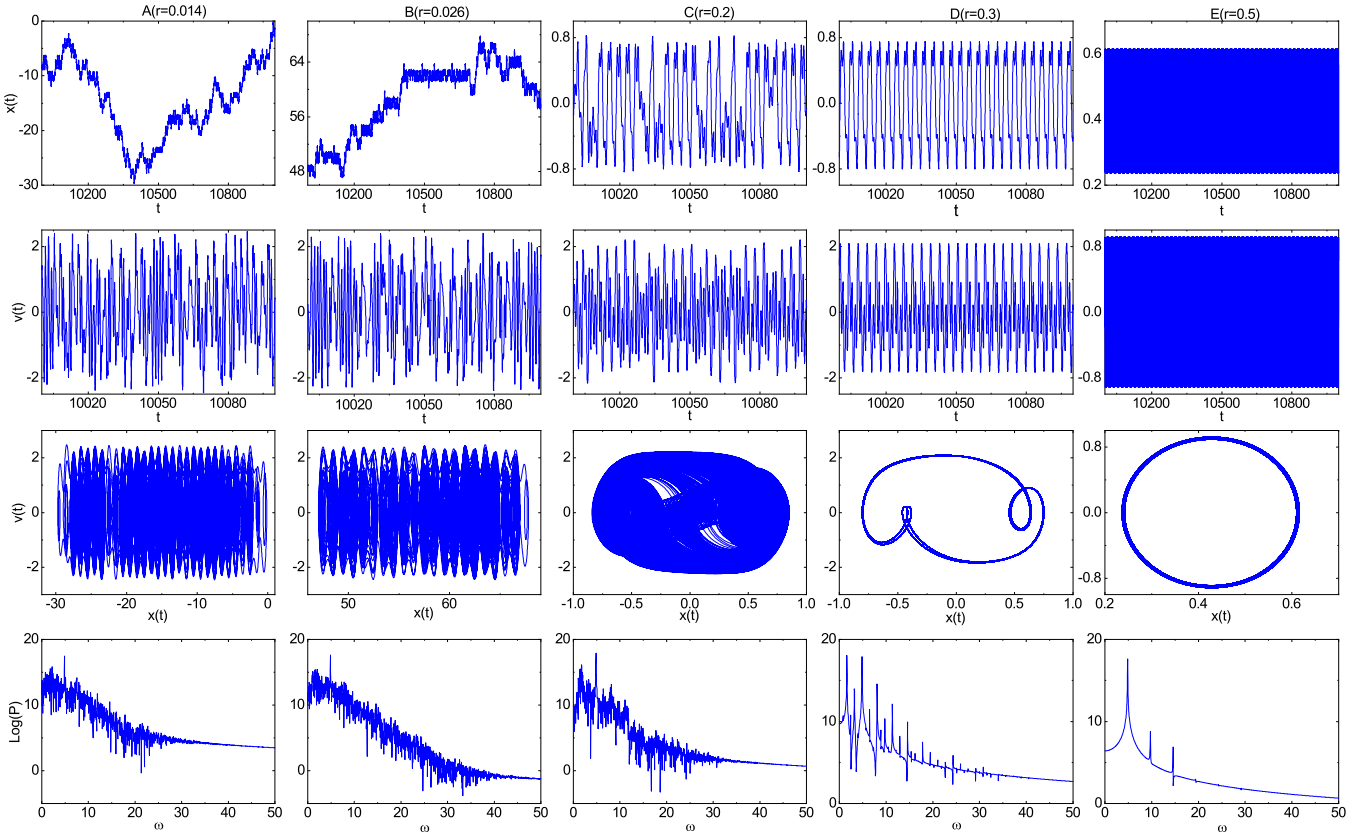

FIG. 3. The time series of position (the first row) and velocity (the second row), phase-space map (the third row), and power spectra (the fourth row) of the noiseless system ($D = 0$) in the presence of shape parameters $r = 0.014$ (the A column), 0.026 (the B column), 0.2 (the C column), 0.3 (the D column), and 0.5 (the E column) that correspond to the points A–E in Fig. 2(a), respectively. The other parameter is $F = 0.05$.

direction of the axis x. This behavior implies that a nontrivial mobility arises in the positive direction. Second, the time series of velocity shows irregularity. Third, the map shows that the trajectory of the particle leaves the initial double well, also called a stable attractor, and continuously forms new unstable attractors in other adjacent double wells in the positive direction of the axis x. Notice that the unstable attractor may be independent of the initial double well, and the next-nearest-neighbor hoppings of the particle for the steady-state result in the appearances of new unstable attractors and nonzero mobilities. Finally, the spectrum is dominated by downward spikes. As a consequence, these results demonstrate that the attractors corresponding to $r = 0.026$ are of SCAs. Additionally, the average velocity corresponding to $r = 0.026$ in Fig. 2(a) is positive, suggesting that the SCAs can cause positive mobility. Let us take a closer look at the lifetimes of unstable attractors for SCAs. The lifetimes of unstable attractors for $r = 0.014$ span from several to decade dimensionless time units, while that for $r = 0.026$ span from several to over 200 dimensionless time units. This means that the firing times of $r = 0.026$ is longer than that of $r = 0.014$. Similar firing times were discussed in recent work [37]. When $r = 0.2$, the C column shows that the time series are irregular, the map covers the phase and trajectories concentrate near the stable equilibrium, and the spectrum has both upward and downward spikes. Thus the attractor corresponding to $r = 0.2$ is of weak chaotic attractor (WCA) [34]. Additionally, the average velocity corresponding to $r = 0.2$ is zero in Fig. 2(a), implying that the average velocity corresponding to WCA is zero. The chaotic bands of WCA are those exactly mentioned above that do not lead to a nonzero mobility. Namely, the attractors corresponding to the small and positive MLE do not lead to negative mobility. When $r = 0.3$, the D column shows that the time series are quasiperiodic, the map displays a torus structure, and the spectrum has peaks and both upward and downward spikes. Therefore, the attractor corresponding to $r = 0.3$ is quasiperiodic. Moreover, the $\langle v \rangle$ corresponding to $r = 0.3$ is zero in Fig. 2(a), implying that quasiperiodic attractor does not result in nonzero mobility. When $r = 0.5$, the E column shows that the time series display periodic behaviors, the map shows period-1 in the positive direction of the axis x, and the power spectrum possesses peaks at discrete frequencies. Therefore the attractor is periodic. Furthermore, the average velocity corresponding to $r = 0.5$ is zero in Fig. 2(a). This finding suggests that periodic attractor does not lead to nonzero mobility. In brief, these results suggest that SCAs can lead to nonzero mobilities which may include anomalous mobility, whereas both nonchaotic attractor and WCA do not result in them. Therefore, now we can answer the question of why certain chaos can give rise to negative or positive mobility, whereas the rest does not. Our results suggest that the SCAs can lead to the emergence of nonzero average velocity, whereas both WCA and nonchaotic attractor do not result in them.

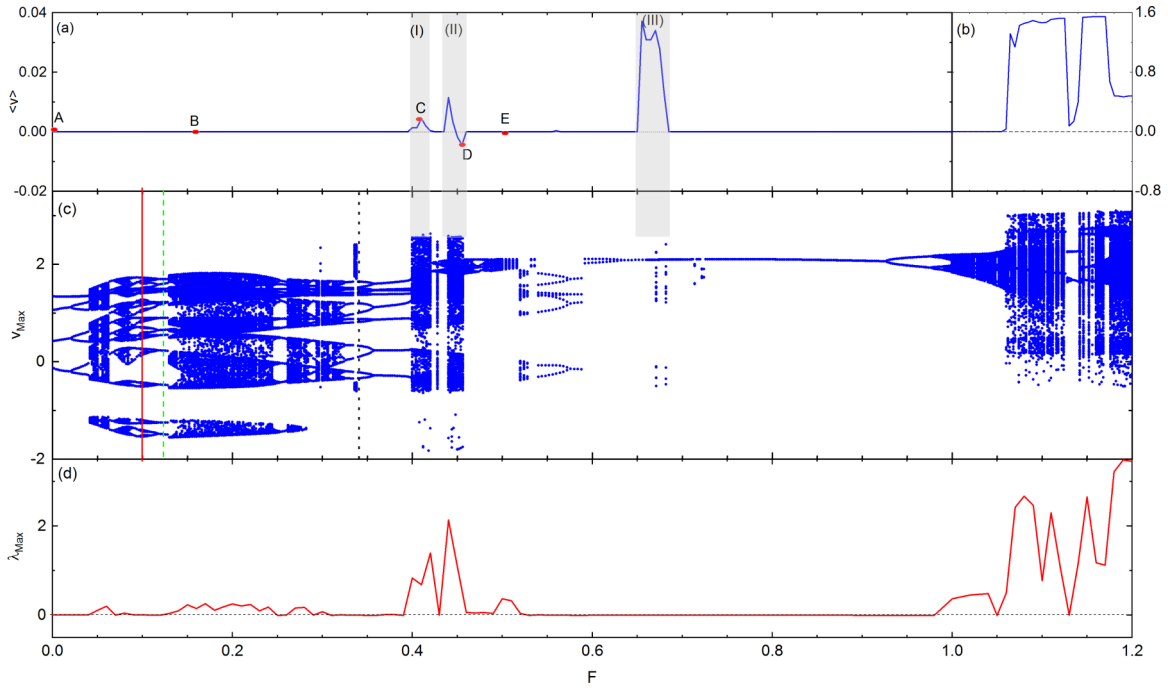

FIG. 4. The average velocity [(a) and (b)], the bifurcation diagram (c), and the MLE (d) vs. the bias F in the absence of noise ($D = 0$). The other parameter is $r = 0.05$. The points A–E referenced in Fig. 5. Moreover, the solid red line, dashed green line, and dotted black line of panel (c) indicating $F = 0.1$, 0.122, and 0.34, which are referenced in Figs. 10–12.

To see how the bias affects the mobility of the particle, we present the average velocity, the bifurcation diagram, and the MLE versus the bias in Fig. 4. The average velocity as the bias F ranging from 0.000 to 1.000 is plotted in Fig. 4(a), which shows that the average velocities are zero except for three ranges of $F = 0.400$ to 0.415 (range I), $F = 0.440$ to 0.455 (range II), and $F = 0.655$ to 0.668 (range III). It should be noted that negative mobility occurs in the range F from 0.450 to 0.455. Additionally, the average velocity as a function of the bias F ranging from 1.00 to 1.20 is presented in Fig. 4(b), which shows that the average velocity is zero for $F < 1.06$, yet positive for $F > 1.06$. Through the comparison between this and Fig. 4(a), it is found that the positive average velocities for $F > 1.06$ is 40 times larger than those of $F < 1.0$. It is of great importance that the varying bias causes negative mobility, DNM and giant positive mobility (GPM).

Figure 4(c) shows that with varying the bias, dynamics of the system exhibits rich dynamical behaviors, such as double-periodic bifurcations, periodic windows, attractor-merging crisis, and chaotic bands. Regime (I) of the occurrence of positive mobilities clearly corresponds to the chaotic band in the bandwidth range of $F = 0.400$ to 0.415. Regime (II) of appearance of nonzero average velocity corresponds to the chaotic band in the bandwidth range of $F = 0.440$ to 0.455. Regime (III) of the emergence of positive mobilities, including DNM and GPM, clearly corresponds to several chaotic points. The reason why it is not chaotic band will be discussed below. Finally, Fig. 4(c) also shows that the varying bias can induce the occurrence of a transition between a nonchaotic band and a chaotic band that may result in the appearance of the negative mobility.

Figure 4(d) shows the MLE λ_{Max} as a function of the bias F. The comparison between Figs. 4(a) and 4(d) reveals that ranges (I) and (II) of the appearance of nonzero average velocities almost correspond to the large and positive MLEs. This finding reveals that chaos can cause the nonzero mobility. However, range (III) of $\langle v \rangle \neq 0.0$ corresponds to $\lambda_{\mathrm{Max}} \simeq 0$. In fact, this behavior suggest that chaos is sensitive to the variation of initial conditions. For certain ranges of the system's parameters, different initial conditions lead to different dynamical behaviors, such as nonchaotic and chaotic behaviors. Here the data of the single trajectory (whose initial position and velocity are 0.1 and 0.0, respectively) are used to plot bifurcation diagram and to calculate the MLE, whereas the average velocity is calculated through 500 trajectories with different initial positions and velocities. In our simulation, average velocity for the time average well matches the results of the bifurcation diagram or the MLE for the same trajectory. These results suggest that for the certain system parameter, certain initial condition make the system evolve in chaotic state, whereas other conditions can induce the evolution of the system in nonchaotic state.

To better understand these dynamical behaviors, we present the time series, the phase-space map, and the power spectrum for different biases in Fig. 5, of which columns A–E correspond to points A–E of Fig. 4(a), respectively. When $F = 0.00$ (the A column), the corresponding time series, phase-space map, and spectrum suggest that the attractor is periodic. This behavior implies that the average velocity corresponding to $F = 0.00$ is zero, which is in agreement with that of Fig. 4(a). When $F = 0.16$ (the B column), the time series, map, and spectrum suggest that the attractor corresponding to $F = 0.16$ is of WCA. Thus, the average velocity corresponding to $F = 0.16$ is nearly zero, which agrees with that of Fig. 4(a). It should be noted that the phenomenon that the velocity direction of the particle is against the small bias is

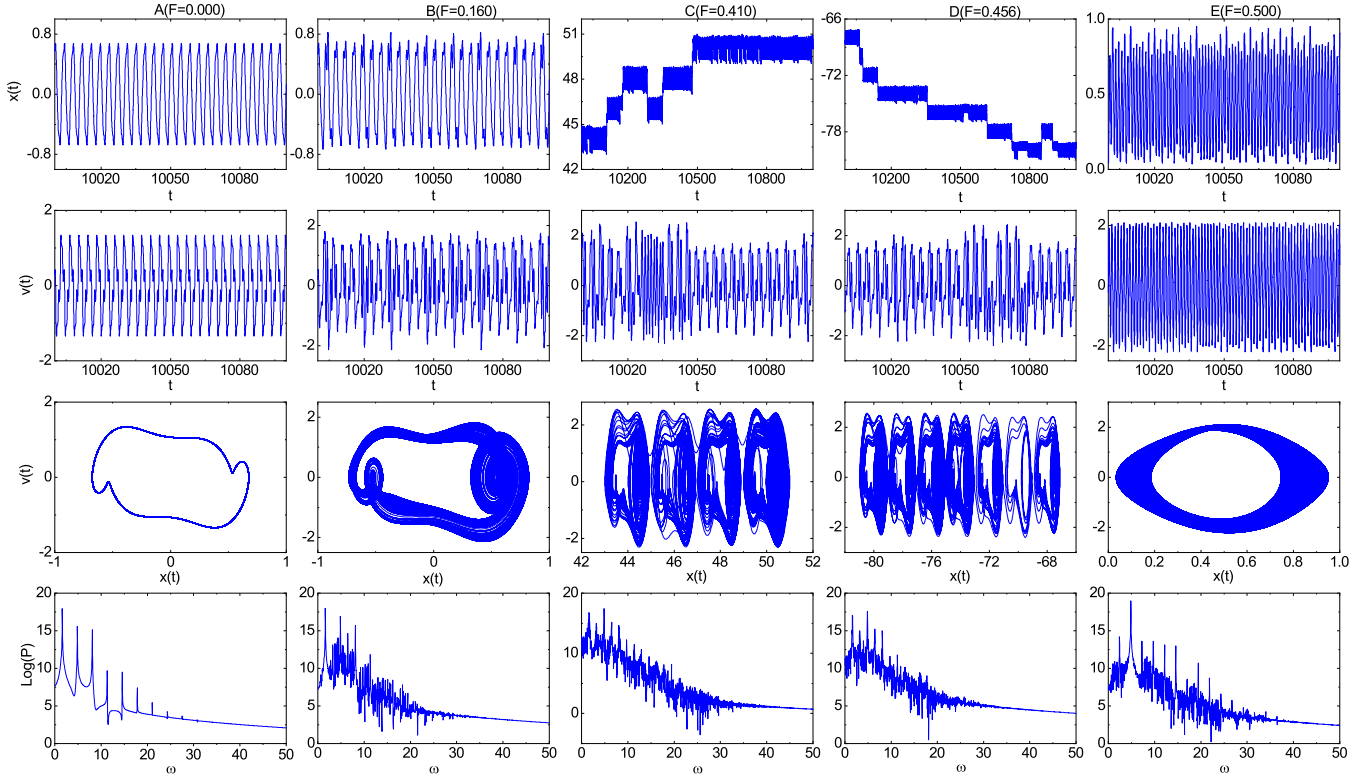

FIG. 5. The time series of position (the first row) and velocity (the second row), phase-space map (the third row), and power spectra (the fourth row) of the noiseless system ($D = 0$) in the absence of the bias $F = 0.000$ (the A column), and in the presence of biases $F = 0.160$ (the B column), 0.410 (the C column), 0.456 (the D column), and 0.500 (the E column) that correspond to the points A–E in the top panel of Fig. 4, respectively. The other parameter is $r = 0.05$.

fascinating. Namely, for a small positive bias (e.g., $F = 0.16$), the time series of the velocity and phase-space map are lightly biased toward the negative direction of velocity (the B column). However, the time series of the position shows that the particle does not leave the initial double well, suggesting that no mobility emerges for $F = 0.16$. When $F = 0.41$ (the C column), the time series, the map, and the spectrum reveal that the attractor is of SCAs in the positive direction of the axis x. This implies that the average velocity corresponding to $F = 0.41$ is positive, which is consistent with that of Fig. 4(a). Moreover, the lifetimes of these unstable attractors span from 70 to over 500 dimensionless time units. The comparison between this and Fig. 3 reveals that these lifetimes are longer than those of Fig. 3. For $F = 0.456$ (the D column), the time series, the map, and the spectrum suggest that the attractors corresponding to $F = 0.456$ are of SCAs in the negative direction of the axis x, revealing the existence of negative mobility, which is in agreement with that of Fig. 4(a). Additionally, the lifetimes of these unstable attractors span from dozens to over 200 dimensionless time units. For $F = 0.5$, the E column shows that the time series, the map, and the spectrum imply that the attractor corresponding to $F = 0.5$ is of a WCA. This finding implies that the corresponding average velocity is zero, which is in agreement with that of Fig. 4(a).

Such an unexpected behavior that the small bias (e.g., $F = 0.410$ or 0.456) can drive the motion of the particle, whereas the large bias (e.g., $F = 0.500$) does not is an interesting character of the dynamics in the potential. The reason is that certain small biases F correspond to SCAs, whereas certain large biases correspond to WCA or nonchaotic attractor. Our simulation suggests that these nonzero mobilities observed are caused by SCAs instead of WCA or nonchaotic attractor. Surely, larger bias (i.e., $F > 1.06$) can drive the motion of the particle in the system, but there still exists the nonlinear response regime, such as NDM in Fig. 4(b). Moreover, when the effect of the potential is negligible for larger bias, the system exhibits linear response.

Results for the dependence of the average velocity on the amplitude a are displayed in Fig. 6, showing the average velocity, the bifurcation diagram, and the MLE versus the amplitude a. Figure 6(a) shows that average velocities are zero except for two ranges of $a = 3.36$ to 4.28 and $a = 5.62$ to 6.15. It must also be mentioned that there exist three times nontrivial negative mobilities with increasing the amplitude a (gray). These findings suggest that the time-periodic force can drive the system out of equilibrium that may result in the occurrence of some paradoxical situations, such as negative mobility. To understand the physical mechanism behind these findings, we analyze these phenomena through the bifurcation diagram of the velocity in Fig. 6(b), which shows that the dynamics of the system exhibits various striking behaviors, such as double-periodic bifurcations, chaotic bands, periodic windows, and attractor-merging crisis. It is of great importance to note that the regimes of the occurrence of nonzero average velocity clearly correspond to certain chaotic bands.

We further demonstrate these results by the MLE in Fig. 6(c), which shows that the chaotic bands in Fig. 6(b)

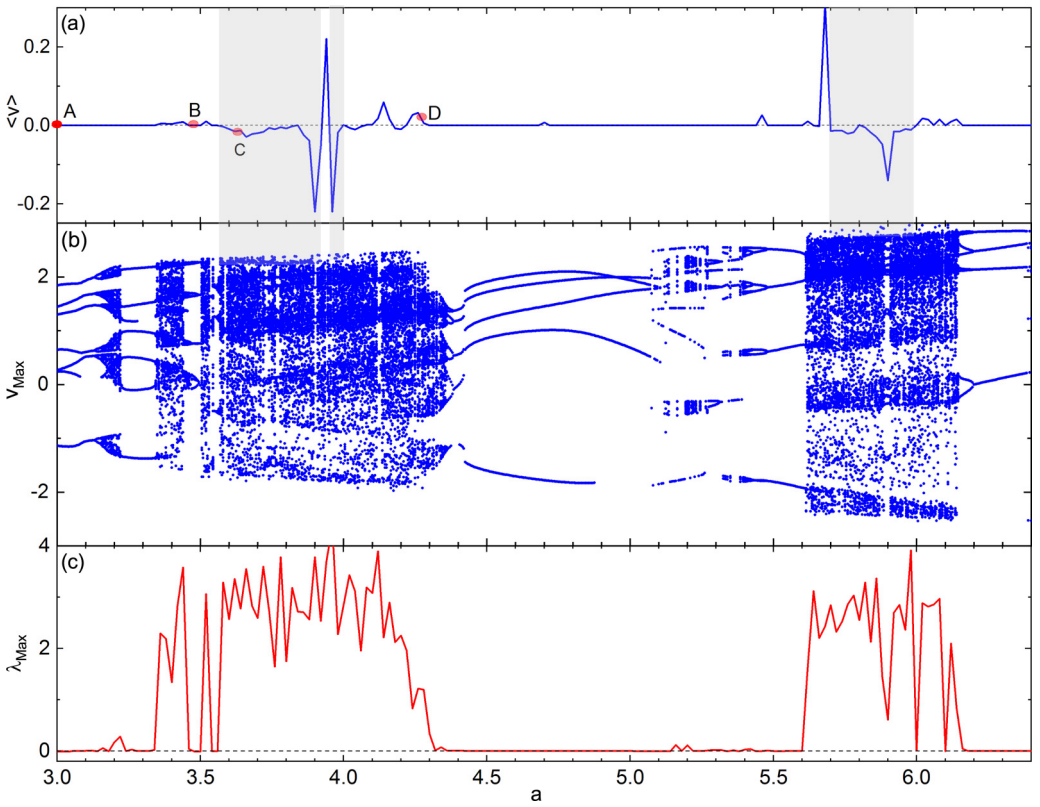

FIG. 6. The average velocity (a), the bifurcation diagram (b), and the MLE (c) vs. the amplitude a in the absence of noise ($D = 0$). The other parameters are $r = 0.05$ and $F = 0.05$. The points A–D referenced in Fig. 7.

clearly correspond to the positive MLE in Fig. 6(c). Moreover, the nonzero average velocities in Fig. 6(a) correspond to the large and positive MLE, whereas the $\langle v \rangle = 0.0$ correspond to $\lambda_{\mathrm{Max}} \simeq 0$ or the small and positive MLEs. Therefore, the result unambiguously demonstrates that these nonzero mobilities, including negative and positive mobilities, are caused by certain chaos.

To elucidate the negative mobility of the particle, we analyze the above findings via the time series, the phase-space map, and the power spectrum in Fig. 7, of which columns A–D indicate the points A–D of Fig. 6(a). When $a = 3.00$ (the A column), the corresponding time series, phase-space map, and power spectrum suggest that the attractor corresponding to $a = 3.00$ is periodic. Consequently, the average velocity corresponding to $a = 3.00$ is zero. For $a = 3.48$ (the B column) in a periodic window, the corresponding time series, map, and power spectrum reveal that the attractor corresponding to $a = 3.48$ is of nonchaotic attractor. This result implies that the average velocity corresponding to $a = 3.48$ is zero. For $a = 3.64$ (the C column), the time series, the map, and the spectrum demonstrate that the attractors corresponding to $a = 3.64$ are of SCAs in the negative direction of the axis x, signaling that SCAs may result in negative mobility. Furthermore, the lifetimes of these unstable attractors span from dozens to over 100 dimensionless time units. For $a = 4.28$ (the D column), the corresponding time series, phase-space map, and power spectrum suggest that there are SCAs in the positive direction of the axis x, indicating the emergence of a positive mobility. These mobilities agree with those of Fig. 6(a). Moreover, we find, from the time series of the position (the D column), that lifetimes of these unstable attractors span from several to dozens dimensionless time units.

To understand how the angular frequency ω affects the transport of the particle, we present the average velocity, the bifurcation diagram, and the MLE versus ω in Fig. 8. We find that there are several ranges of the occurrence of nonzero average velocity in Fig. 8(a). It should be noted that there are seven times negative mobilities with increasing ω in the figure. We also find that these nonzero mobilities in Fig. 8(a) clearly correspond to certain chaotic bands in Fig. 8(b). We also prove these findings by the MLE, namely the nonzero mobilities in Fig. 8(a) clearly correspond to the large and positive MLE in Fig. 8(c). These results suggest that strong chaos can cause nonzero mobilities.

To better understand the diffusions of the particle corresponding to various dynamical behaviors, we present mean-square displacement (MSD) and time-dependent diffusion coefficient (TDDC) in Fig. 9. Here the MSD and the TDDC are defined by [6] $\langle \Delta x^2(t) \rangle = \langle x^2(t) \rangle - \langle x(t) \rangle^2$ and $D(t) = \langle \Delta x^2(t) \rangle / (2t)$, respectively. Here $\langle\rangle$ denotes the ensemble average including 10^4 trajectories. Notice that the case where $D(t)$ increases with time is superdiffusion, whereas the case where $D(t)$ decreases with time denotes subdiffusion. Additionally, $D(t) = \text{const}$ represents normal diffusion. In general, normal diffusion corresponds to $\langle \Delta x^2(t) \rangle \propto t^1$, suggesting that $D(t) = \text{const}$ denotes effective diffusion coefficient.

The MSD and TDDC as functions of time for different r are plotted in Fig. 9(a) and 9(d), respectively, whose parameters

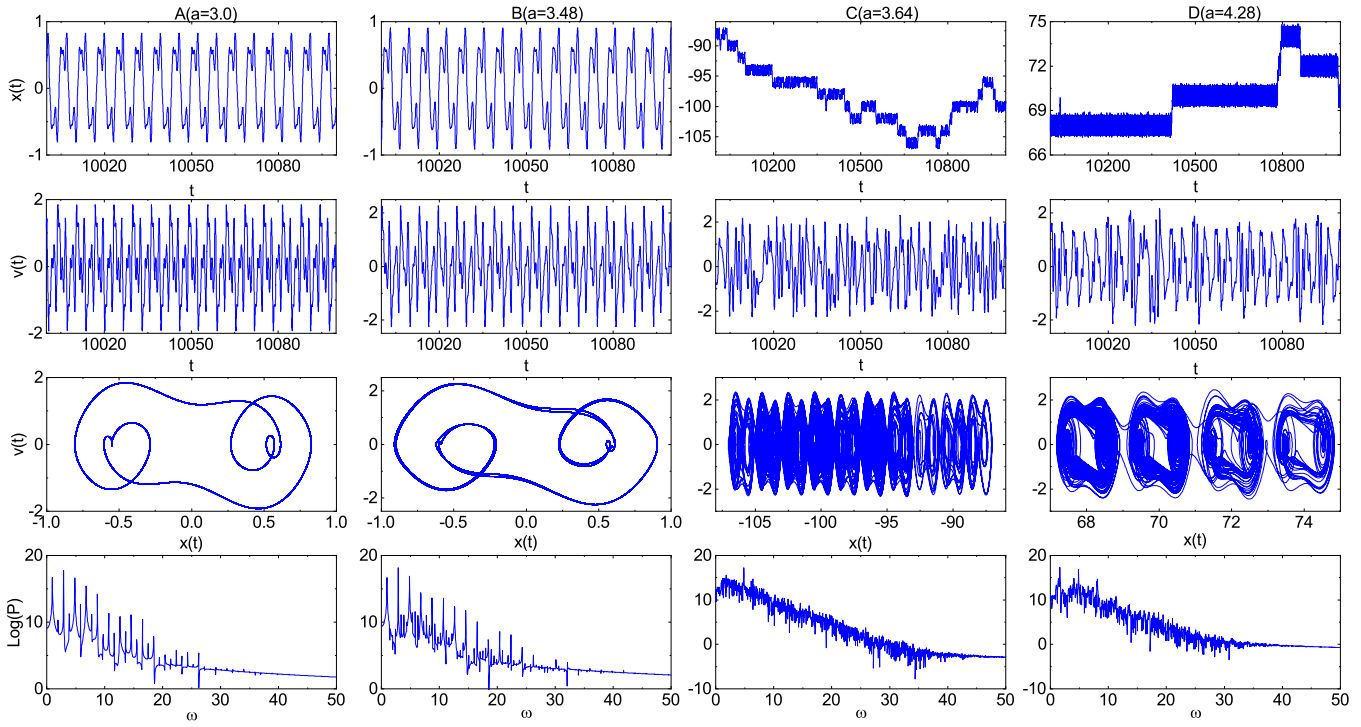

FIG. 7. The time series of position (the first row) and velocity (the second row), phase-space map (the third row), and power spectra (the fourth row) of the noiseless system ($D = 0$) for different the amplitudes a. The columns A, B, C, and D correspond to $a = 3.00$, 3.48, 3.64, and 4.28, respectively, which denote points A–D in the top panel of Fig. 6. The other parameters are $r = 0.05$ and $F = 0.05$.

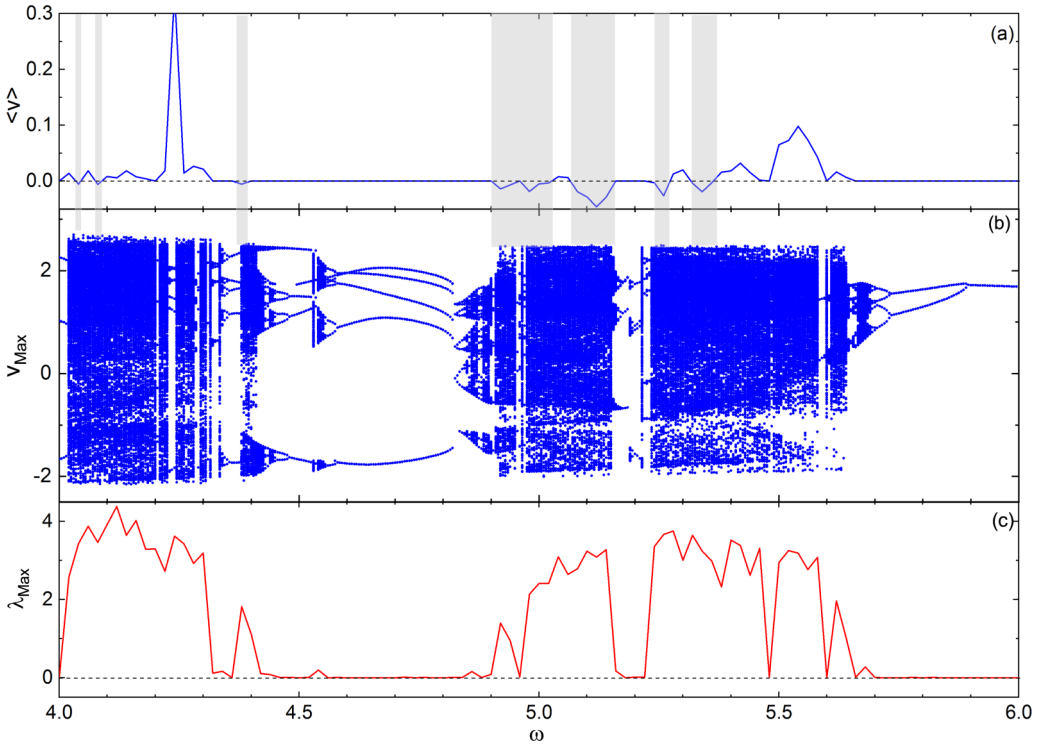

FIG. 8. The average velocity (a), the bifurcation diagram (b), and the MLE (c) vs. the angular frequency ω in the absence of noise ($D = 0$). The other parameters are $r = 0.05$ and $F = 0.05$.

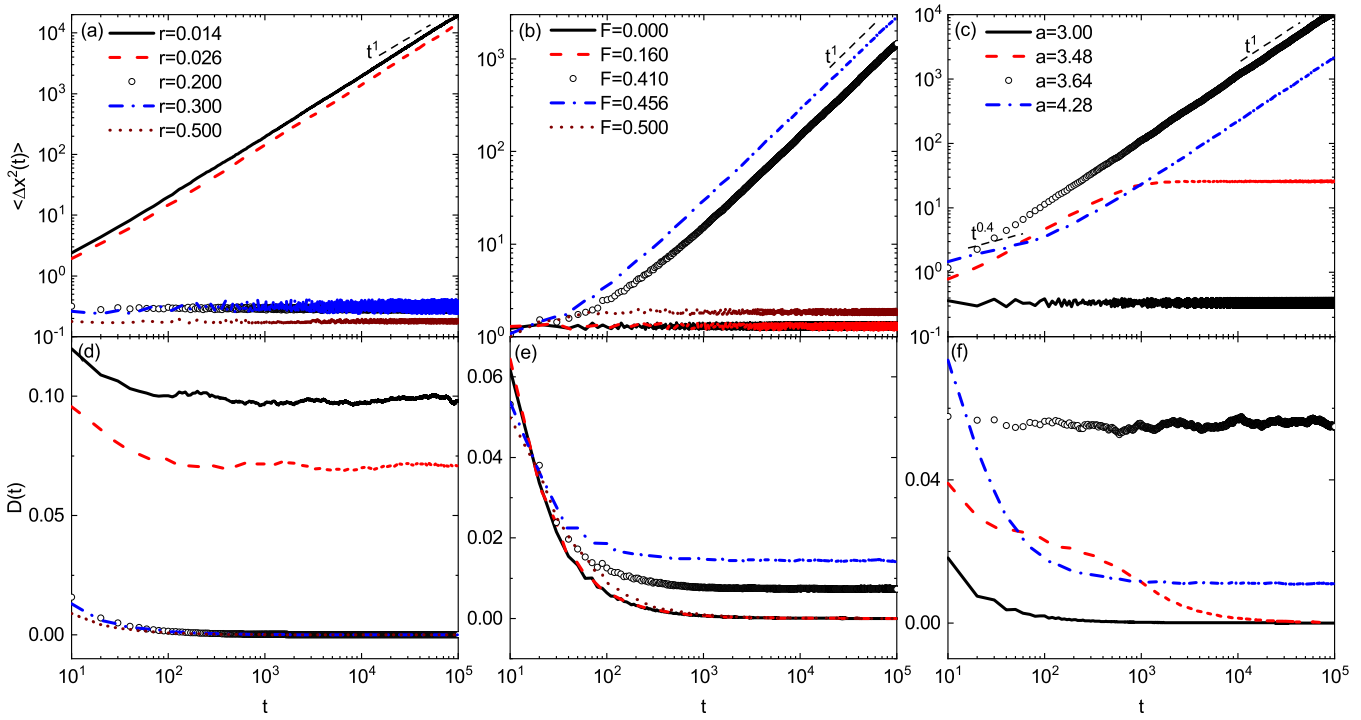

FIG. 9. The mean-square displacement and time-dependent diffusion coefficient. The other parameters of (a) and (d) are the same as those of Fig. 3, the other parameters of (b) and (e) are the same as those of Fig. 5, and the other parameters of (c) and (f) are the same as those of Fig. 7.

are same as those of Fig. 3. When $r = 0.014$ (the solid black curve) and 0.026 (the dashed red curve), the MSDs scale as t^1 on long timescales, suggesting that the diffusions are normal on long timescales in Fig. 9(d). For $r = 0.2$ (the black circle curve), 0.3 (the dashed- and dotted-blue curve), and 0.5 (the short dashed dark red curve), the MSDs trivially oscillate with time. These behaviors suggest that the particle remains in the initial double well. As a result, there is no diffusion, shown in Fig. 9(d).

The MSD and TDDC as functions of time for different F are plotted in Figs. 9(b) and 9(e), respectively, whose parameters are same as those of Fig. 5. When $F = 0.000$ (the solid black curve), 0.160 (the dashed red curve), and 0.500 (the short dashed dark red curve), the MSDs trivially oscillate with time, suggesting that the particle does not leave the initial double well. Namely, the diffusions are zero [Fig. 9(e)]. For $F = 0.410$ (the black circle curve) and 0.456 (the dashed-and-dotted blue curve), the MSDs scales as t^1 on long timescales. These behaviors suggest that the diffusions are normal [Fig. 9(e)].

The MSD and TDDC as functions of time for different a are plotted in Figs. 9(c) and 9(f), respectively, whose parameters are same with those of Fig. 7. When $a = 3.00$ (the solid black curve), the MSD and TDDC suggest that there is no diffusion, as shown in Figs. 9(c) and 9(f). For $a = 3.48$ (the dashed red curve), the MSD increases with time first and then becomes trivially oscillation with time. This behavior suggest that the particle hoppings from a double well to another double well in initial transient state, whereas it remains in a double well in steady state. As a result, the particle undergoes subdiffusion on short timescales, and then zero diffusion occurs on long timescales in Fig. 9(f). When $a = 3.64$ (the black circle curve), the MSD scales as t^1 on long timescales, and thus the particle undergoes normal diffusion, which is proven by TDDC in Fig. 9(f). For $a = 4.28$, The MSD scales as $t^{0.4}$ on short time interval and as $t^{1.0}$ on long timescales, (the dashed-and-dotted blue curve) namely the particle undergoes subdiffusion first and then normal diffusion [Fig. 9(f)]. Based on the above, we find that there is no diffusion for WCA and nonchaotic attractor for the steady state, whereas various diffusions may appear for SCAs in different intervals. This finding suggests that strong chaos may result in the coexistence of various diffusions and negative mobility.

B. The presence of the Gaussian color noise

To understand the effect of a Gaussian color noise, we study the mobilities of the particle moving in the potential with a Gaussian color noise in Figs. 10–13. Figure 10(a) illustrates the average velocity as a function of the bias F in the presence of the color noise for different values of r. For small or large shape parameters (e.g., $r = 0.0$ or 0.1), no clear ANM is observed, whereas ANM arises for the suitable r (e.g., $r = 0.05$). This behavior can be explained as follows. Figure 2(a) shows that $r = 0.0$ and 0.1 are far from chaotic bands, although there are perturbations of both noise and the bias, chaos does not arise in these regimes. But $r = 0.05$ is nearby a chaotic band, and thus the presence of perturbations (e.g., the bias, noise) can induce the emergence of the transition from a nonchaotic attractor to SCAs. This transition implies that the transition from zero to nonzero average velocity, which may include negative mobility, occurs. We also

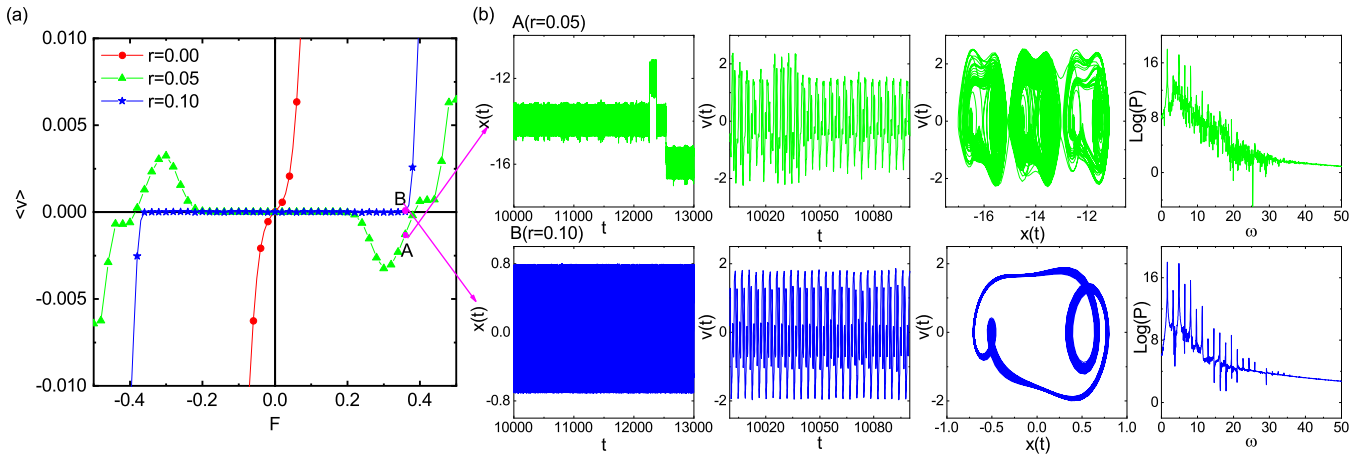

FIG. 10. The averaged velocity $\langle v \rangle$ versus the bias F for different shape parameters r (a), and the time series of position and velocity, the phase-space map, and the power spectra of points A ($r = 0.05$) and B ($r = 0.10$) with $F = 0.34$ (b), respectively. The other parameters are $\tau_0 = 1.0$ and $D = 0.001$.

analyze the physical mechanism of these phenomena through the time series, the phase-space map, and the power spectrum in Fig. 10(b), of which rows A and B correspond to points A and B of Fig. 10(a), respectively. When $r = 0.05$ (the A row), the time series, the map, and the spectrum suggest that the attractors corresponding to $r = 0.05$ are SCAs in the negative direction of the axis x. The occurrence of the SCAs implies that anomalous transport of ANM occurs, in agreement with that of Fig. 10(a). Moreover, the firing times of these unstable attractors span from dozens to over 2000 dimensionless time units. Finally, this finding can be regarded as the consequence of a nonchaotic attractor, labeled by the dotted black line in Fig. 4 ($F = 0.34$), that is perturbed by a Gaussian color noise. Namely, a Gaussian color noise can induce the occurrence of a transition from a nonchaotic attractor to SCAs, implying that the transition from zero to negative mobility occurs. For $r = 0.10$ (the B row), the time series, the map, and the spectrum suggest that the attractor corresponding to $r = 0.10$ is of WCA, implying that the corresponding average velocity is zero. The result is consistent with that of Fig. 10(a). Thus these results suggest that the shape parameter r is of great importance for the appearance of anomalous mobility.

For further understanding of the role of the Gaussian color noise, the dependence of the anomalous mobility on the noise intensity D and the correlation time τ_0 are plotted in Figs. 11 and 12, respectively. Figure 11(a) shows that for different D, the transports of the particle display different behaviors. For weak noise intensity (e.g., $D = 10^{-3}$ and 10^{-2}), ANM and GPM coexist, whereas GPM almost eliminates and ANM remains for strong noise intensity (e.g., $D = 10^{-1}$). These findings are analyzed via the time series, the phase-space map, and the power spectrum for different D in Fig. 11(b), of which rows A–C correspond to points A–C of Fig. 11(a), respectively. For $D = 10^{-3}$ (the A row),

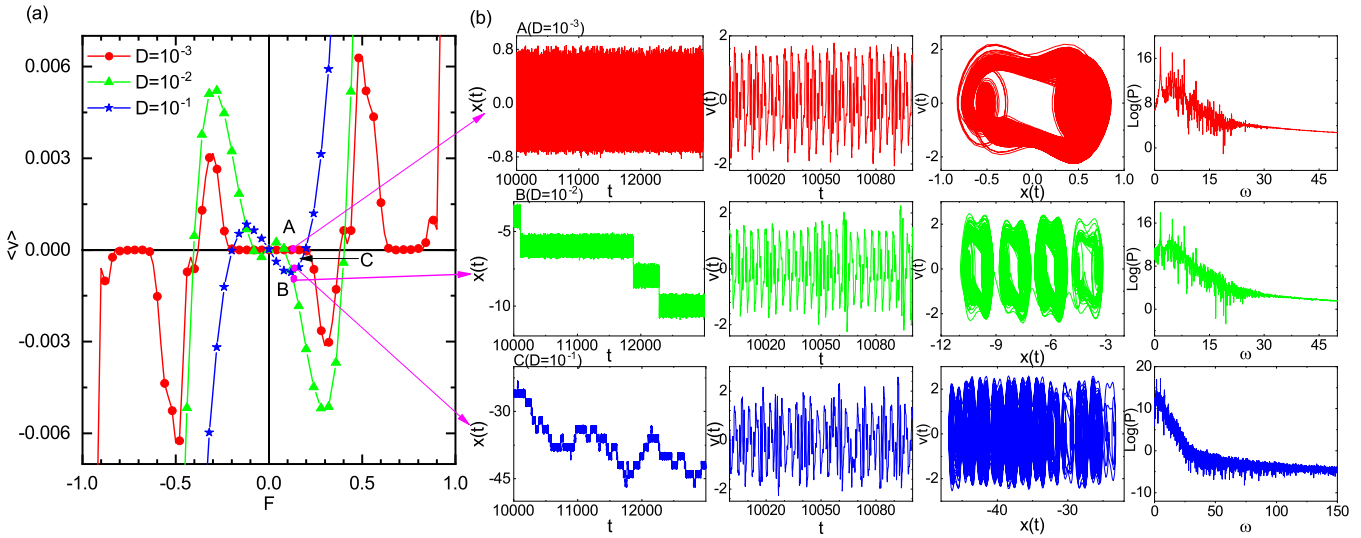

FIG. 11. The averaged velocity $\langle v \rangle$ versus the bias F for different noise intensities D (a), and the time series of position and velocity, the phase-space map, and the power spectra of the system in the presence of noise intensities $D = 10^{-3}$ (the A row), $D = 10^{-2}$ (the B row), and $D = 10^{-1}$ (the C row) that correspond to points A–C with $F = 0.122$ (b), respectively. The other parameters are $\tau_0 = 1.0$ and $r = 0.05$.

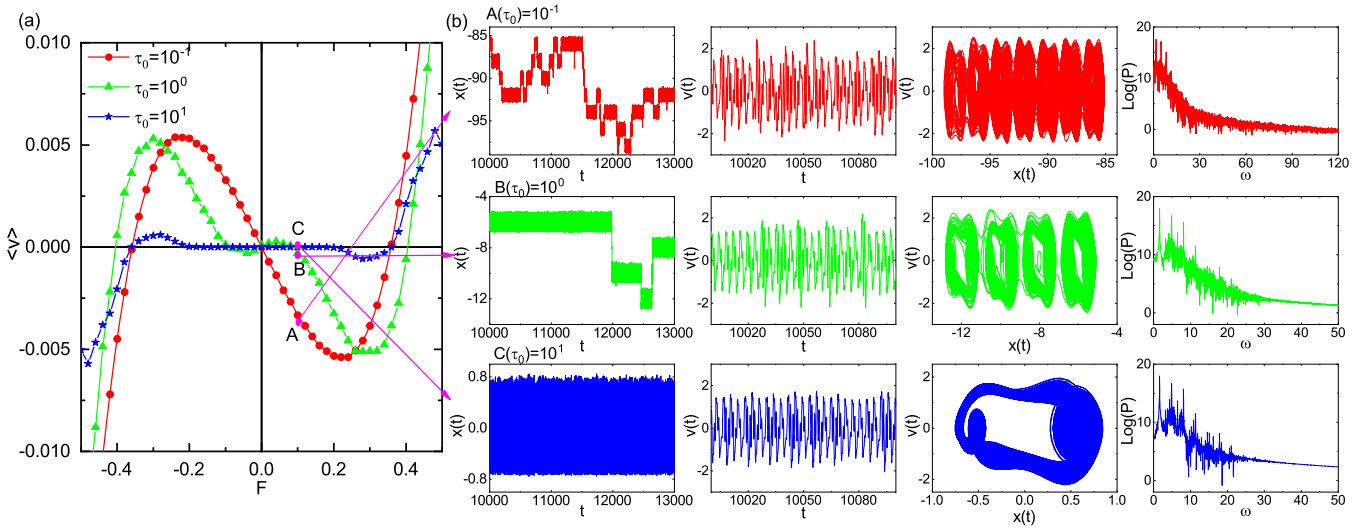

FIG. 12. The averaged velocity $\langle v \rangle$ versus the bias F for different correlation times τ_0 (a), and the time series of position and velocity, the phase-space map, and the power spectra of the noise system in the presence of correlation times $\tau_0 = 0.1$ (the A row), $\tau_0 = 1.0$ (the B row), and $\tau_0 = 10$ (the C row) that correspond to points A–C with $F = 0.1$ (b), respectively. The other parameters are $D = 0.01$ and $r = 0.05$.

the time series, the map, and the power spectrum suggest that the attractor corresponding to $D = 10^{-3}$ is of WCA, indicating that the average velocity corresponding to $D = 10^{-3}$ is zero. The result is in agreement with that of Fig. 11(a). When $D = 10^{-2}$ (the B row), the time series, the map, and the spectrum suggest that the attractors corresponding to $D = 10^{-2}$ are SCAs in the negative direction of the axis x, implying that ANM occurs. The result is in agreement with that of Fig. 11(a). Additionally, the lifetimes of these unstable attractors span from decade to almost 2000 time units. For $D = 10^{-1}$ (the C row), the time series, the map, and the power spectrum suggest that the attractors corresponding to $D = 10^{-1}$ are also SCAs in the negative direction of the axis x, revealing that ANM occurs. This result well matches that of Fig. 11(a). The significant difference between $D = 10^{-1}$ and $D = 10^{-2}$ is the lifetimes of these unstable attractors. The lifetimes of unstable attractors corresponding to $D = 10^{-1}$ span from several to hundreds of time units, which is nearly 10 times shorter than that of $D = 10^{-2}$. Finally, these results can be regarded as the consequences of a nonchaotic attractor, labeled by the dashed green line in Fig. 4 ($F = 0.122$), that is perturbed by a Gaussian color noise. We find that the particle stays its initial double well and forms a stable attractor when the noise intensity D is smaller than a threshold value. When

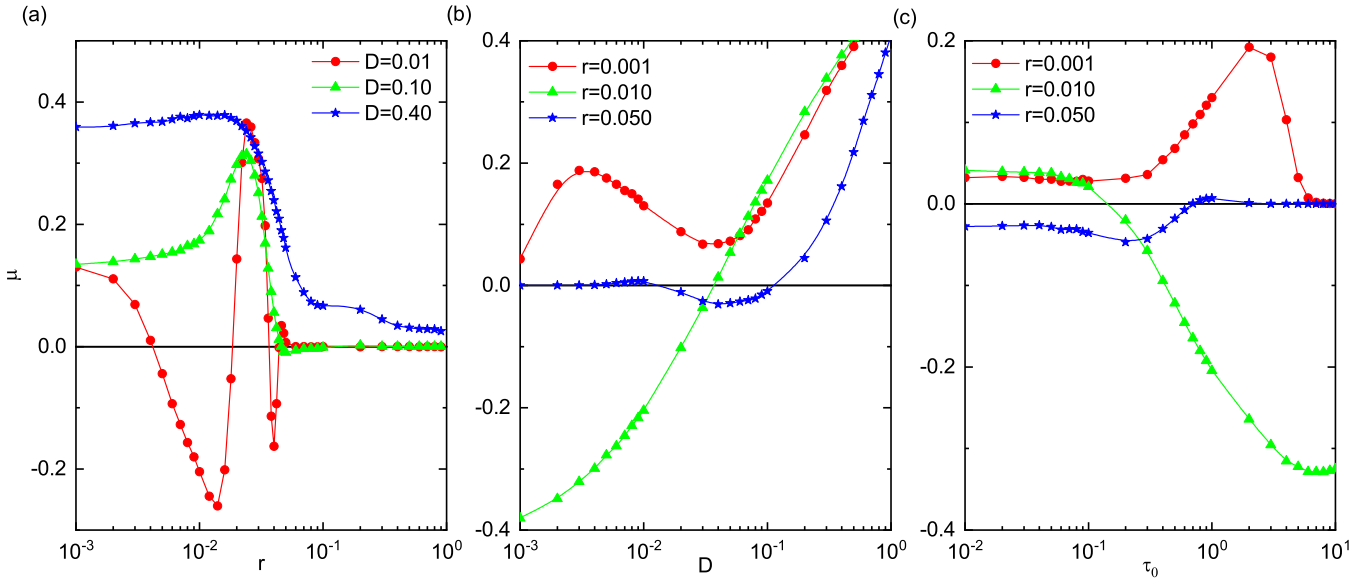

FIG. 13. (a) The mobility coefficient μ versus shape parameter r for different noise intensities D with $\tau_0 = 1.0$. (b) The mobility coefficient μ versus noise intensity D for different shape parameters r with $\tau_0 = 1.0$. (c) The mobility coefficient μ versus correlation time τ_0 for different shape parameters r with $D = 0.01$.

the noise intensity exceeds the threshold value, the particle leaves the initial double well, implying that the anomalous mobilities and unable attractors may arise. Additionally, the lifetimes of these unable attractors decrease on increasing the noise intensity D above the threshold value. In a word, noise intensity can lead to the occurrence of the transition from a nonchaotic attractor to SACs nearby chaotic bands. The transition implies that there exists the appearance of the transition from zero to nonzero mobility including negative or positive mobility. Namely, the noise may lead to the emergence of negative mobility.

We now turn to the effects of the correlation time. The average velocity as a function of the bias F for different τ_0 is presented in Fig. 12(a). At $\tau_0 = 0.1$, clear ANM is observed, while there coexists significant ANM and trivial GPM at $\tau_0 = 1.0$. However, GPM vanishes, and ANM is weakened at $\tau_0 = 10.0$. It is also shown that the peak of ANM produces a shift when changing τ_0. Subsequently, the increase in τ_0 can weaken ANM. Therefore, the results suggest that the increasing correlation time τ_0 can weaken, even eliminate ANM. To better understand the correlation time effect on the transport of the particle, we analyze these findings via the time series, the phase-space map, and the power spectrum in Fig. 12(b), of which rows A–C correspond to point A–C of Fig. 12(a), respectively. When $\tau_0 = 0.1$ (the A row), the time series, the phase-space map, and the power spectrum suggest that the attractors corresponding to $\tau_0 = 0.1$ are SCAs in the negative direction of the axis x. These SCAs implies that ANM arises, also in agreement with that of Fig. 12(a). For $\tau_0 = 1.0$ (the B row), the time series, the phase-space map, and the power spectrum suggest that the attractors corresponding to $\tau_0 = 1.0$ are also SCAs in the negative direction of the axis x, revealing that there exits an ANM. The result also matches that of Fig. 12(a). For $\tau_0 = 10.0$ (the C row), the time series, the phase-space map, and the power spectrum suggest that the corresponding attractor is of WCA. The WCA implies that the corresponding average velocity is zero, in agreement with that of Fig. 12(a). Moreover, their time series of the position show that lifetimes of these unable attractors increase with increasing the correlation time first. Second, the particle stays the initial double well and negative mobility vanishes when correlation time exceeds a critical value. Finally, these results can be regarded as the consequences of a nonchaotic attractor, labeled by the solid red line in Fig. 4 ($F = 0.1$), that is perturbed by a Gaussian noise. We find that a transition from a nonchaotic attractor to SCAs occurs in presence of a Gaussian color noise with $\tau_0 = 0.1$. Subsequently, the anomalous mobilities are weakened and the lifetimes of these unable attractors increase on increasing the correlation time. Additionally, the anomalous mobilities vanish on increasing the correlation time τ_0 above a critical value. Based on the above results, it is shown that the correlation time can weaken and even eliminate chaotic behaviors, implying that the increasing correlation time can weaken and even eliminate the negative mobility.

To gain a better understanding of the underlying anomalous mobility, we study the mobility of the particle via the mobility coefficient below. Here the mobility coefficient is defined by $\mu = \frac{\partial \langle v \rangle}{\partial F}|_{F=0}$ [4]. Notice that $\mu < 0$ denotes that the particle works against the small bias, suggesting that $\mu < 0$ is anomalous mobility. On the contrary, $\mu > 0$ represents that the velocity of the particle is positive for positive load, vice versa, suggesting that $\mu > 0$ is normal mobility. We plot the mobility coefficients μ versus the shape parameter r, noise intensity D, and correlation time τ_0 in Fig. 13. The figure shows that there are double ANMs and GPMs with varying r for $D = 0.01$, while there is one ANM and GPM with increasing r for $D = 0.1$. But ANM disappears and there exists a trivial GPM with increasing r for $D = 0.4$. To gain more insight, we plot the mobility coefficient as a function of noise intensity and correlation time for different r in Figs. 13(b) and 13(c), respectively. Figure 13(b) shows that as the noise intensity increases, there exists DNM at $r = 0.001$, while at $r = 0.01$, the particle firstly undergoes GPM and then becomes ANM and, finally, positive mobility. Moreover, the transition from negative to positive mobility occurs with increasing the noise intensity D at $r = 0.05$. Figure 13(c) shows that as the correlation time increases, positive mobility increases first and then decreases and becomes zero for $r = 0.001$ finally, while for $r = 0.01$, there exists the transition from positive to negative mobility. Finally, the particle undergoes negative mobility first and then becomes positive mobility and zero mobility with increasing the correlation time at $r = 0.05$.

Based on the above, the results suggest that the SCAs can result in anomalous mobility and that the dynamical behavior is sensitive to the variations of the shape parameter r, the noise intensity D, and the correlation time τ_0. The physical mechanism of the phenomenon is that a small perturbation can lead to a transition between a nonchaotic attractor and a chaotic attractor in certain parameters' regimes. The chaotic dynamical behavior is known to be sensitive to the variation of the control parameters of the system. Therefore, the transition from a chaotic attractor to a nonchaotic attractor may result in the transition from a nonzero mobility to a zero mobility. On the contrary, the transition from the nonchaotic attractor to the chaotic attractor may lead to the transition from a zero mobility to a nonzero mobility. This is the physical mechanism that the Gaussian color noise induce the occurrence or disappearance of the anomalous mobility.

IV. CONCLUDING REMARKS

Taken together, we numerically investigate negative mobility of an inertial Brownian particle moving in a periodic double-well substrate potential driven by a time-periodic force and a constant bias for the deterministic dynamics and the presence of a color thermal fluctuation. For the deterministic dynamics, we find from the average velocity that certain system parameters or driving forces can induce the occurrence of the negative mobility. Moreover, it is clear from the bifurcation diagram and the MLE that certain chaos can lead to nonzero mobilities which may include the negative mobility, whereas the rest does not. Relative results were demonstrated in the cosine like type potentials which exhibit anomalous transport induced by transient chaos [38,39]. To better understand the physical mechanisms underlying these findings, we mainly analyze them via SCAs, WCA, and nonchaotic attractors and find that SCAs can cause the negative mobility, whereas WCA and periodic and quasiperiodic attractors do not.

For the presence of the Gaussian color noise, it is revealed that the noise may give rise to a transition from a type of attractor to another since chaotic dynamical behavior is known to be sensitive to the variation of both the initial conditions and the system's parameters. When the transition to SCAs arises, it implies that the negative mobility may arise. Our simulation findings suggest that the noise intensity results in the existence of the negative mobility, while the correlation time may result in its disappearance.

In brief, our results unveil how the phenomena of the anomalous mobility connect to SCAs including both stable attractor and unstable attractors that may directly lead to the occurrence of negative mobility. Our findings may be potentially useful for research on anomalous transports of the particles, and on the designs of various circuits, such as circuits of atomic chains, Chua's circuit, charge-density-wave conductors, Josephson junctions arrays, devices of crystals with dislocations, hydrogen-bonded networks, and superconducting nanowires.

ACKNOWLEDGMENTS

We thank the referees for their constructive comments. This work was supported by the National Natural Science Foundation of China (Grants No. 11665014 and No. 12075090), the Yunnan Fundamental Research Projects (Grant No. 2019FI002), the Key-Area Research and Development Program of Guang Dong Province (Grant No. 2019B030330001), the Yunnan Ten Thousand Talents Plan Young & Elite Talents Project, and Science and Technology Program of Guangzhou (Grant No. 2019050001).

[1] T. Salger, S. Kling, T. Hecking, C. Geckeler, L. Morales-Molina, and M. Weitz, Directed transport of atoms in a hamiltonian quantum ratchet, Science **326**, 1241 (2009).

[2] M. D. Pierro, D. A. Potoyan, P. G. Wolynes, and J. N. Onuchic, Anomalous diffusion, spatial coherence, and viscoelasticity from the energy landscape of human chromosomes, Proc. Natl. Acad. Sci. USA **115**, 7753 (2018).

[3] A. Purkayastha, A. Dhar, and M. Kulkarni, Nonlinear transport in an out-of-equilibrium single-site bosehubbard model: Scaling, rectification, and time dynamics, Phys. Rev. A **94**, 052134 (2016).

[4] L. Machura, M. Kostur, P. Talkner, J. Łuczka, and P. Hänggi, Absolute Negative Mobility Induced by Thermal Equilibrium Fluctuations, Phys. Rev. Lett. **98**, 040601 (2007).

[5] J. Spiechowicz and J. Łuczka, Josephson phase diffusion in the superconducting quantum interference device ratchet, Chaos **25**, 053110 (2015).

[6] J. Spiechowicz, P. Hänggi, and J. Łuczka, Coexistence of Absolute Negative Mobility and Anomalous Diffusion, New J. Phys. **21**, 083029 (2019)

[7] R. Eichhorn, P. Reimann, and P. Hänggi, Brownian Motion Exhibiting Absolute Negative Mobility, Phys. Rev. Lett. **88**, 190601 (2002).

[8] D. Speer, R. Eichhorn, and P. Reimann, Directing Brownian Motion on a Periodic Surface, Phys. Rev. Lett. **102**, 124101 (2009).

[9] B. S. Dandogbessi and A. Kenfack, Absolute negative mobility induced by potential phase modulation, Phys. Rev. E **92**, 062903 (2015).

[10] P. C. Bressloff and J. M. Newby, Stochastic models of intracellular transport, Rev. Mod. Phys. **85**, 135 (2013).

[11] A. Słapik, J. Łuczka, P. Hänggi, and J. Spiechowicz, Tunable Mass Separation Via Negative Mobility, Phys. Rev. Lett. **122**, 070602 (2019).

[12] J. Wang, G. Casati, and G. Benenti, Inverse Currents in Hamiltonian Coupled Transport, Phys. Rev. Lett. **124**, 110607 (2020).

[13] Y. Luo and C. Zeng, Negative friction and mobilities induced by friction fluctuation, Chaos **30**, 053115 (2020).

[14] Y. F. He, B. Q. Ai, C. X. Dai, C. Song, R. Q. Wang, W. T. Sun, F. C. Liu, and Y. Feng, Experimental Demonstration of a Dusty Plasma Ratchet Rectification and its Reversal, Phys. Rev. Lett. **124**, 075001 (2020).

[15] J. C. Wu, T. W. Dong, G. W. Jiang, M. An, and B. Q. Ai, Particle separation induced by triangle obstacles in a straight channel, J. Chem. Phys. **152**, 034901 (2020).

[16] A. Ros, R. Eichhorn, J. Regtmeier, T. T. Duong, P. Reimann, and D. Anselmetti, Absolute negative particle mobility, Nature **436**, 928 (2005).

[17] K. L. Chong, J.-Q. Shi, G.-Y. Ding, S.-S. Ding, H.-Y. Lu, J.-Q. Zhong, and K.-Q. Xia, Vortices as brownian particles in turbulent flows, Sci. Adv. **6**, eaaz1110 (2020).

[18] J. Zhang and T. Önskog, Langevin equation elucidates the mechanism of the Rayleigh-Bénard instability by coupling molecular motions and macroscopic fluctuations, Phys. Rev. E **96**, 043104 (2017).

[19] J. Zhang, P. Tian, S. Yao, and F. Fei, Multiscale investigation of kolmogorov flow: From microscopic molecular motions to macroscopic coherent structures, Phys. Fluids **31**, 082008 (2019).

[20] A. K. Chatterjee, U. Basu, and P. K. Mohanty, Negative differential mobility in interacting particle systems, Phys. Rev. E **97**, 052137 (2018).

[21] A. Słapik, J. Łuczka, and J. Spiechowicz, Negative mobility of a brownian particle: Strong damping regime, Commun. Nonlin. Sci. Numer. Simulat. **55**, 316 (2018).

[22] M. Remoissenet and M. Peyrard, Soliton dynamics in new models with parameterized periodic double-well and asymmetric substrate potentials, Phys. Rev. B **29**, 3153 (1984).

[23] D. Yemélé and T. C. Kofané, Low-temperature statistical mechanics of kink-bearing systems with a Remoissenet-Peyrard substrate potential: Influence of anharmonic interactions, Phys. Rev. B **72**, 054301 (2005).

[24] B. Hu and J. Tekić, Dynamical mode locking in commensurate structures with an asymmetric deformable substrate potential, Phys. Rev. E **72**, 056602 (2005).

[25] S. Pnevmatikos, Soliton Dynamics of Hydrogen-Bonded Networks: A Mechanism for Proton Conductivity, Phys. Rev. Lett. **60**, 1534 (1988).

[26] J. Tekić, P. Mali, Z. Ivić, and M. Pantić, Size effect of the subharmonic Shapiro steps on the interference phenomena in the Frenkel-Kontorova model with realistic substrate potentials, J. Appl. Phys. **114**, 174504 (2013).

[27] O. M. Braun and Y. S. Kivshar, Nonlinear dynamics of the Frenkel-Kontorova model, Phys. Rep. **306**, 1 (1998).

[28] Y. Lachtioui, A. Kotri, I. Tarras, K. Saadouni, and M. Mazroui, Substrate effects on the diffusion process, Mol. Cryst. Liq. Cryst. **628**, 86 (2016).

[29] S. B. Yamgoué and T. C. Kofané, Dynamics of driven coupled oscillators with shape deformable potential, Chaos Solitons Fract. **15**, 119 (2003).

[30] J. Tekić and B. Hu, Properties of the shapiro steps in the ac driven Frenkel-Kontorova model with deformable substrate potential, Phys. Rev. E **81**, 036604 (2010).

[31] B. Q. Ai and B. Hu, Heat conduction in deformable Frenkel-Kontorova lattices: Thermal conductivity and negative differential thermal resistance, Phys. Rev. E **83**, 011131 (2011).

[32] E. Coquet, M. Remoissenet, and P. T. Dinda, Oscillations of a highly discrete breather with a critical regime, Phys. Rev. E **62**, 5767 (2000).

[33] M. Kostur, J. Łuczka, and P. Hänggi, Negative mobility induced by colored thermal fluctuations, Phys. Rev. E **80**, 051121 (2009).

[34] Y. Suzuki, M. Lu, E. Ben-Jacob, and J. N. Onuchic, Periodic, quasi-periodic and chaotic dynamics in simple gene elements with time delays, Sci. Rep. **6**, 21037 (2016).

[35] R. L. Honeycutt, Stochastic Runge-Kutta algorithms. ii. Colored noise, Phys. Rev. A **45**, 604 (1992).

[36] A. Wolf, J. B. Swift, H. L. Swinney, and J. A. Vastano, Determining lyapunov exponents from a time series, Physica D **16**, 285 (1985).

[37] H.-L. Zou, Z.-C. Deng, W.-P. Hu, K. Aihara, and Y.-C. Lai, Partially unstable attractors in networks of forced integrate-and-fire oscillator, Nonlin. Dyn. **89**, 887 (2017).

[38] D. Speer, R. Eichhorn, and P. Reimann, Brownian motion: Anomalous response due to noisy chaos, Europhys. Lett. **79**, 10005 (2007).

[39] D. Speer, R. Eichhorn, and P. Reimann, Transient chaos induces anomalous transport properties of an underdamped brownian particle, Phys. Rev. E **76**, 051110 (2007).